The use of basis splines and non-orthogonal orbitals in *R*-matrix calculations: application to Li photoionization

2000 J. Phys. B: At. Mol. Opt. Phys. 33 313

(http://iopscience.iop.org/0953-4075/33/3/303)

J. Phys. B: At. Mol. Opt. Phys. **33** (2000) 313–341. Printed in the UK PII: S0953-4075(00)06334-3

The use of basis splines and non-orthogonal orbitals in R-matrix calculations: application to Li photoionization

Oleg Zatsarinny† and Charlotte Froese Fischer‡

† Institute of Electron Physics, Academy of Science, Uzhgorod 294016, Ukraine
‡ Vanderbilt University, Box 1679B, Nashville, TN 37235, USA

Received 26 July 1999, in final form 18 November 1999

Abstract. We present a new extended version of the R-matrix method for the calculation of continuum properties in which non-orthogonal orbitals are extensively used for describing both the target states and the R-matrix basis functions. In particular, a B-spline basis is used for the description of continuum states in the inner region and the target states may be obtained from independent calculations. This leads to a generalized eigenvalue problem but has the advantage of requiring much smaller bases for accurate representation of target wavefunctions and to achieve convergence in the close-coupling expansion. The present approach and its code are both applicable to a general atom and their efficiency for low-energy scattering processes is demonstrated by calculating the photoionization of Li. A detailed analysis of the resonance structure is given. Very good agreement with experimental data has been obtained, and considerable improvement in the description of resonances has been achieved in comparison with the standard R-matrix calculations.

1. Introduction

The R-matrix technique describing electron and photon scattering by complex atoms and ions was first introduced by Burke *et al* (1971) and now is among the most widely applied methods for the determination of various atomic properties. The compilation volume by Burke and Berrington (1993) includes the major papers in R-matrix theory along with a comprehensive list of calculations using the method.

In fact, the R-matrix method is one of many methods for solving the standard close-coupling equations. The important difference with the straightforward close-coupling formalism (Burke and Seaton 1971) is a separate treatment of the two regions in phase space: an inner region, in which all the electrons are fully interacting with each other and eventual external fields, and an outer region, in which the outer electron only feels a local potential. Here the coupled equations (without exchange) are solved for each collision energy and matched, at the boundary $r = a$, to the solution in the inner region. However, instead of solving a set of coupled integro-differential equations in the internal region for each collision energy, the $(N + 1)$-electron wavefunction is expanded in terms of an energy-independent basis set and treated as similarly as possible to the treatment of N electrons in general complex atom or ion bound states. Consequently, general computer codes written for bound-state atomic structures can be used, with only slight modifications, to generate the scattering algebra.

In practice, all existing codes use one common set of orthogonal one-electron radial functions for representing the target states, which simplifies the computations considerably. A weakness of this method is that it is difficult to achieve an accurate representation for all target states, especially, in the case of the core excitation. The continuum orbitals are

0953-4075/00/030313+29$30.00

also assumed to be orthogonal to all bound orbitals. This can cause difficulties in the case of unphysical pseudo-orbitals which need to be used for a more accurate representation of the target wavefunctions, and special procedures have been developed for a separate treatment of orthogonality constraints with respect to physical and pseudo-orbitals (Bartschat 1998). Another problem due to these orthogonality conditions arises from the fact that for completeness of the total trial function the close-coupling expansion has to also contain the bound part consisting of certain $(N+1)$-electron configurations which are routinely constructed from scattering wavefunctions by replacing continuum orbitals with bound ones. It may drastically increase the size of the interaction matrix, but the main problem is the appearance of pseudo-resonance structures in the excitation cross sections (see, for example, the discussion by Gorczyca *et al* (1995)). The authors suggest a procedure for elimination of some pseudo-resonances by additional transformations of the bound portion of the scattering wavefunction, but this procedure is not general and cannot be fully automated.

The use of the non-orthogonal orbital technique can overcome the above problems in a standard application of the R-matrix method. The use of non-orthogonal orbitals was avoided because of the fact that the most time-consuming part of atomic structure calculations is connected with the angular integration of the Hamiltonian matrix elements. A set of efficient general codes had been developed for this task in the case of fully orthogonal orbitals (Hibbert 1970, Hibbert *et al* 1991) or with some restricted non-orthogonality (Hibbert and Froese Fischer 1991). They allowed one to automate to a large extent the R-matrix calculations and resulted in widespread application of this method. With the appearance of efficient codes for dealing with non-orthogonal orbitals in a general way (Zatsarinny 1996, Zatsarinny and Froese Fischer 1999), it became possible to use any non-orthogonal basis in the atomic structure calculations. One of the main tasks of the present work is to introduce this non-orthogonality technique into the R-matrix method and to analyse its efficiency.

Another purpose of the present work is to examine employing B-splines as the effective R-matrix basis in the inner region. B-splines are bell-shaped piecewise polynomial functions, of order k_s (degree $k_s - 1$), and are completely defined given the order and a set of points (knot sequence) which may be in part coincident and divide the radial interval $[0, R]$ into adjacent subintervals. The mathematical properties of B-splines are fully described in a monograph by de Boor (1985) which also contains FORTRAN algorithms for the construction and manipulation of B-splines. B-splines were introduced into atomic structure calculations only a few years ago, but became widely used due to their excellent numerical approximation properties (for reference see topical papers by Hansen *et al* (1993), Sapirstein and Johnson (1996)). Much less effort has been made to use B-splines for continuum states. The first tests for simple systems, such as the free electron or the Coulomb equation, were done by Froese Fischer and Idrees (1989). The method determines the required solution on the B-spline basis within a finite boundary, with no assumed boundary condition. This approach has been further generalized to the single- and multichannel continuum case, mainly with application to photoionization of few-body systems such as H, He, H^- and He^- (Brage *et al* 1992, Venuti and Decleva 1997, Xi and Froese Fischer 1999). The method can be referred to as a straightforward method for solving the close-coupling equations when the solution over the whole configuration space is searched at each given energy point.

The important property of B-splines is that they form a *complete* basis for piecewise polynomials of order $k - 1$ on the interval spanned by the knot sequence. The characteristic feature of B-splines is that the Schrödinger equation is solved within a box, which is very similar to the inner region in the R-matrix method, and it can be expected that B-splines will be very effective for forming the R-matrix basis. The first and only attempt to employ B-splines in R-matrix theory has been done by van der Hart (1997) for scattering on one-electron

atoms, and excellent agreement was found with the benchmark results for this simple system. B-splines form the non-orthogonal basis, and a further extension of the proposed method to many-electron systems needs an extensive use of the non-orthogonal technique. One such extension is proposed in the present work.

1s photoionization of Li has been chosen as a benchmark test for the proposed R-matrix technique. From a theoretical point of view, the case of a three-electron system is an excellent choice. The study of photoionization processes of small atoms can be carried out using accurate theoretical treatments and therefore a better understanding of both the electronic structure of the target and the dynamics of the process can be obtained. On the other hand, the availability of accurate experimental results enables the theoretical models to be tested in a detailed way. Although Li is the simplest open-shell system, the photoionization process is already complex, since the Li^+ ion can be left in several excited states, and understanding the lithium spectra is an important first step to the understanding of more complicated systems.

Many approaches have been pursued in the study of Li photoionization and a good estimate for the quality of a computational method can be obtained from a detailed comparison. In this respect, we can mention the recent extensive calculations in the standard R-matrix approach using the 11-state (Lisini *et al* 1990) and 19-state (Vo Ky *et al* 1998) target expansions, and very accurate calculations of resonance structure by Chung (1997a, b) using the saddle-point complex-rotation method. Furthermore, photoionization spectra of Li were recently measured (Kiernan *et al* 1996) with a very high energy resolution ($E/\Delta E \cong 10\,000$), by using a dilute atomic beam of lithium with monochromatized vacuum-ultraviolet synchrotron radiation, and this provides us with another important comparison.

2. Method

In this section we first summarize the basic equations that arise in low-energy scattering theory in order to provide a framework for the analysis and comparison of the present method, given in the rest of this paper, for the example of calculation of photoionization of Li.

Most computational methods describing low-energy collisions start from an expansion of the total wavefunction in terms of target states Φ_i as

$$\Psi = A \sum_i \Phi_i(x_1, \ldots, x_N) F_i(x_{N+1}) + \sum_i \chi_i(x_1, \ldots, x_{N+1}) c_i \tag{1}$$

where $x_i \equiv \boldsymbol{r}_i \sigma_i$ represents the space and spin coordinates of the ith electron and the operator A here includes antisymmetrization as well as relevant angular coupling. The first summation in equation (1) goes over a finite number of target eigenstates and possible pseudostates, and the second expansion goes over a set of square-integrable (L^2) correlation functions χ_i which allow for electron–electron correlation effects not adequately represented by the limited number of terms which can be retained in the first expansion. The expansion (1) is usually referred to as a close-coupling expansion.

Coupling equations for the radial components of the functions $F_i(x)$ representing scattered electrons and the coefficients c_i can be obtained by substituting expansion (1) into the Schrödinger equation and projecting onto target functions Φ_i and onto L^2 functions χ_i. After separating out the spin and angular variables and eliminating the coefficients c_i we obtain the following set of coupled integro-differential equations:

$$\left(\frac{\mathrm{d}^2}{\mathrm{d}r^2} - \frac{l_i(l_i+1)}{r^2} + \frac{2dZ}{r} + k_i^2\right) F_i(r) = 2 \sum_j (V_{ij} + W_{ij} + X_{ij}) F_j(r) \tag{2}$$

satisfied by the radial components $F_i(r)$. In this equation, l_i is the orbital angular momentum of the scattered electron and V_{ij}, W_{ij} and X_{ij} are the partial-wave decompositions of the local direct, non-local exchange and non-local correlation potentials. These potentials are too complicated to write down explicitly except for the simplest atoms. Instead they are constructed by general computer programs. The equations can also contain terms which arise from the orthogonality constraints on the scattering radial functions $F_i(r)$.

A set of different computational methods for solving equations (2) to yield the scattering matrices and amplitudes, which can be compared with experiment, has been developed over the last few decades. These methods now form the basis of a number of computer program packages, some of which are widely used. As an example, we can mention the linear algebraic equation method (Crees *et al* 1978), the non-iterative integral equation method (Henry *et al* 1981) and the convergent close-coupling method (Bray and Stelbovics 1995). All of these methods can be referred to as straightforward methods where the solution of equation (2) is obtained in all of configuration space for each collision energy. A promising new approach for the direct solution of the close-coupling equations (2), based on the B-spline basis and notable for its simplicity which is the key to a successful computational implementation, has been put forward recently by Froese Fischer and Idrees (1989). The method determines the required solution within a finite boundary, with no assumed boundary conditions. This is not a limitation, provided that the asymptotic region is reached, so that the solutions can be matching to a linear combination of true asymptotic solutions. The core of the algorithm involves evaluation of the Hamiltonian and overlap matrix elements in the B-spline basis,

$$H_{ij} = \langle \Psi_i, H\Psi_j \rangle \qquad S_{ij} = \langle \Psi_i, \Psi_j \rangle \tag{3}$$

and extraction of the eigenvectors relative to the minimum modulus eigenvalues of the non-Hermitian, energy-dependent matrix

$$A(E) = H - ES \tag{4}$$

at each prefixed energy E. Here the very effective inverse iteration procedure is used.

The important difference of the R-matrix method with the above-mentioned close-coupling formalism is the division of configuration space into two regions, $r \leqslant a$ and $r > a$, where the R-matrix radius a is chosen in such a way that exchange effects between the projectile and the target electrons can be neglected in the external region. Here the coupling equations (with simple long-range potentials) are solved for each collision energy and matched, at the boundary $r = a$, to the solution in the inner region. However, instead of solving a set of coupled integro-differential equations (2) in the internal region for each collision energy, the $(N+1)$-electron wavefunction at energy E is expanded in terms of an *energy-independent* basis set, Ψ_k, as

$$\Psi_E = \sum_k A_{Ek} \Psi_k. \tag{5}$$

The basis states for given total angular momenta are constructed as

$$\Psi_k^\Gamma(x_1, \ldots, x_{N+1}) = A \sum_{ij} \bar{\Phi}_i^\Gamma(x_1, \ldots, x_N; \hat{\boldsymbol{r}}_{N+1}\sigma_{N+1})\, r_{N+1}^{-1}\, u_j(r_{N+1})\, a_{ijk}^\Gamma + \sum_i \chi_i^\Gamma(x_1, \ldots, x_{N+1})\, b_{ik}^\Gamma. \tag{6}$$

The channel functions $\bar{\Phi}_i^\Gamma$ are obtained by coupling the target states with the spin-angular functions of the scattered electron and

$$\Gamma \equiv \alpha L S M_L M_S \pi \tag{7}$$

represents the conserved quantum numbers L and M_L, the total orbital angular momentum and its z component, S and M_S, the total spin angular momentum and its z component, π, the parity, and α, any other quantum numbers required to completely define the channel. We use the LS-coupling scheme and neglect all relativistic effects. The u_i in equation (6) are radial continuum basis functions describing the motion of the scattering electron that are non-zero on the boundary of the internal region. These provide a link between the solution in the internal and external regions. The quadratically integrable functions χ_i^Γ have the same meaning as in equation (1) and are assumed to be fully confined in the internal region.

Consider now the solution of the Schrödinger equation in the internal region. We note that the Hamiltonian H_{N+1} is not Hermitian in this region due to the surface term at $r = a$ that arises from the kinetic energy operators. These surface terms can be cancelled by introducing the Bloch operator

$$L_{N+1} = \sum_{i=1}^{N+1} \tfrac{1}{2}\delta(r_i - a)\left(\frac{\mathrm{d}}{\mathrm{d}r_i} - \frac{b-1}{r_i}\right) \tag{8}$$

where b is an arbitrary constant (in the present implementation we use $b = 0$). $H_{N+1} + L_{N+1}$ is then easily seen to be Hermitian for functions satisfying arbitrary boundary conditions at $r = a$. We then rewrite the Schrödinger equation in the inner region as

$$(H_{N+1} + L_{N+1} - E)\Psi = L_{N+1}\Psi \tag{9}$$

which can be formally solved in terms of the R-matrix basis functions Ψ_k^Γ which are obtained as eigenfunctions of the equation

$$\langle \Psi_i^\Gamma | H_{N+1} + L_{N+1} | \Psi_j^\Gamma \rangle_{\mathrm{int}} = E_i^\Gamma \langle \Psi_i^\Gamma | \Psi_j^\Gamma \rangle_{\mathrm{int}} \tag{10}$$

where the integration over the radial variables in this region is restricted to the internal region. The formal solution of equation (9) can then be expanded as

$$|\Psi^\Gamma\rangle = \sum_k |\Psi_k^\Gamma\rangle \frac{1}{E_k^\Gamma - E} \langle \Psi_k^\Gamma | L_{N+1} | \Psi^\Gamma \rangle_{\mathrm{int}}. \tag{11}$$

Projecting this equation onto the channel functions $\bar{\Phi}_i^\Gamma$ and evaluating on the boundary of the internal region $r_{N+1} = a$ yields

$$F_i^\Gamma(a) = \sum_j R_{ij}^\Gamma(E)\left(a\frac{\mathrm{d}F_j^\Gamma}{\mathrm{d}r} - bF_j^\Gamma\right)_{r_{N+1}=a} \tag{12}$$

where we have introduced the R-matrix

$$R_{ij}^\Gamma(E) = \frac{1}{2a}\sum_k \frac{w_{ik}^\Gamma w_{jk}^\Gamma}{E_k^\Gamma - E} \tag{13}$$

the reduced radial wavefunctions

$$r_{N+1}^{-1} F_i^\Gamma(r_{N+1}) = \langle \bar{\Phi}_i^\Gamma | \Psi^\Gamma \rangle' \tag{14}$$

and the surface amplitudes

$$a^{-1} w_{ik}^\Gamma = \langle \bar{\Phi}_i^\Gamma | \Psi_k^\Gamma \rangle'_{r_{N+1}=a}. \tag{15}$$

The primes on the brackets in equations (14) and (15) mean that the integration is carried out over all the electronic space and spin coordinates except the radial coordinate r_{N+1} of the scattered electron. Equations (12) and (13) are the basic equations describing the scattering

of electrons by atoms or ions in the internal region. Together with the following relations for coefficients A_{Ek} (5):

$$A_{Ek} = \frac{1}{2a}(E_k - E)^{-1} \sum_i w_{ik}(a) \left(a \frac{\mathrm{d}F_i}{\mathrm{d}r} - bF_i \right)_{r=a} = \frac{1}{2a}(E_k - E)^{-1} \boldsymbol{w}^T \boldsymbol{R}^{-1} \boldsymbol{F} \tag{16}$$

they allow us to establish the total wavefunction Ψ_E in the inner region for any value of the total energy E given the values of the scattering orbital on the boundary. The R-matrix given by equation (13) is obtained at all energies by diagonalizing $H_{N+1} + L_{N+1}$ once for each set of conserved quantum numbers Γ to determine the basis functions Ψ_k^Γ and the corresponding eigenenergies E_k^Γ. The logarithmic derivatives of the reduced radial wavefunctions F_i^Γ on the boundary of the internal region are then given by equation (12).

An important point in the R-matrix method is the choice of the radial continuum basis functions u_j in equation (6). Although members of any complete set of functions satisfying arbitrary boundary conditions can be used, a careful choice will enable the convergence of expansion (6) to be more rapid. In the standard R-matrix approach developed by the Belfast group (Berrington *et al* 1995) numerical basis functions satisfying homogeneous boundary conditions at $r = a$ were adopted. This approach gives accurate results provided that corrections proposed by Buttle (1967), to allow for the omitted high-lying poles in the R-matrix expansion, are included. The shortcoming of this approach is that all basis functions have the same (usually, zero) logarithmic derivative at the boundary of the internal region, and it leads to a discontinuity in the slope of the resulting continuum orbitals. In the standard approach, the basis functions u_i are constructed to be orthogonal to the bound orbitals P_{nl} used for the construction of the target wavefunctions. To compensate the arising restrictions on the total wavefunctions, the basis states Ψ_k^Γ must contain the correlation functions χ_i^Γ of the form

$$\chi_i^\Gamma(x_1, \ldots, x_{N+1}) = A\left\{ \bar{\Phi}_i^\Gamma(x_1, \ldots, x_N; \hat{\boldsymbol{r}}_{N+1}\sigma_{N+1})\, r_{N+1}^{-1}\, P_{nl}(r_{N+1}) \right\}. \tag{17}$$

In the case of complex atoms, when extensive many-configuration expansions are used for an accurate representation of target state wavefunctions, this may lead to an extremely large number of correlation functions χ_i^Γ which must be included in the close-coupling expansion for compensation of the orthogonality constraints.

The key point of the present approach is the use of the splines $B_i(r)$ instead of the one-electron basis functions $u_i(r)$ in the R-matrix representation (6) of the inner region. The B-splines possess properties as though they were especially created for the R-matrix theory. They form the complete basis on the final interval $[0, R]$, have a universal nature and are very convenient in numerical calculations because they allow us to avoid finite-difference formulae. Here we have to distinguish between using B-splines as another basis for representation of one-electron orbitals and using B-splines for generating the complete pseudo-spectrum for some one-electron Hamiltonian as in the atomic structure calculations. In the present approach the coefficients a_{ijk} are found from diagonalization (10) of the full Hamiltonian. Up to now, this direct implementation of B-splines in the R-matrix approach was constrained by the fact that the B-splines form a non-orthogonal basis. This considerably complicates the angular algebra. With the appearance of an efficient code (Zatsarinny and Froese Fischer 1999) to deal with the non-orthogonal orbitals in a general way, it becomes possible to use any non-orthogonal basis in atomic structure calculations, and the present approach uses this possibility extensively.

The boundary conditions in the B-spline basis defines only the first and last basis functions which are the only terms different from zero for $r = 0$ and $r_{\max}$, respectively. Boundary conditions for the scattering function at the origin are satisfied, in the form $F(0) = 0$, simply

by removing the first B-spline from the basis set. For definition of the R-matrix at the boundary (13), the amplitudes of the wavefunctions at $r = r_{\max}$, w_{ki}, are required. These values are defined by the coefficients of the last spline which is equal to one at the boundary. The summation over the entire expansion (5) now gives the surface amplitude in a straightforward manner.

The next step in the calculation is to solve the scattering problem in the external region and to match the solutions on the boundary $r = a$ in order to obtain the K-matrices, S-matrices or phase shifts. Since the radius a is chosen such that electron exchange is negligible in this region, the potential in the close-coupling equations are reduced to the multipole expansion in inverse powers of r

$$V_{ij}^{\Gamma}(r) = \sum_{\lambda \geqslant 1} \alpha_{ij}^{\Gamma} r^{-\lambda-1}. \tag{18}$$

The long-range coefficients α_{ij} together with the target energies and the definition of the structure of the close-coupling equations constitute the necessary information needed to solve the scattering problem in the external region. This problem is well developed, and there is a set of general codes for their solution. The most efficient is the outer region program FARM (Burke and Noble 1995) which uses the R-matrix propagator technique. In the present implementation for photoionization of Li, we use the program ASYPCK (Crees 1980) for treating the external region, because for calculation of photoionization cross sections, in addition to the K-matrix, we also need the outer region solutions at the boundary $r = a$. Note that in the outer region we have all the n_0 independent solutions, where n_0 is the number of open channels which are defined by all the target states accessible at a given excitation energy.

In the R-matrix theory, the photoionization cross sections can be defined through the dipole matrix between the initial state Ψ_0 and the R-matrix basis states Ψ_k^{Γ} provided that all radial orbitals of the initial state are well confined in the inner region. The total photoionization cross section for a given photon energy ω is

$$\sigma(\omega) = \left(\tfrac{4}{3}\pi^2 a_0^2 \alpha\right)\left(\frac{\omega C}{2L_0+1}\right)\sum_{j\Gamma} |(\Psi_j^- \| D \| \Psi_0)|^2 \tag{19}$$

where D is a general dipole operator which could be either the length or velocity operator, $C = 1$ in the length form, and $C = 4/\omega^2$ in the velocity form, with the photon energy being in Rydbergs, the index $j = 1, \ldots, n_0$ goes over different possible solutions, and other quantities have their usual meaning. Expanding Ψ_j^- in terms of the R-matrix states as in equation (6) and using the expressions (16), we find that

$$(\Psi_j^- \| D \| \Psi_0) = \frac{1}{a}\sum_k \frac{(\Psi_k \| D \| \Psi_0)}{E_k - E_0 - \omega} \boldsymbol{w}_k^T \boldsymbol{R}^{-1} \boldsymbol{F}_j^-(a) \tag{20}$$

where $(\Psi_k \| D \| \Psi_0)$ are reduced matrix elements between the initial state and R-matrix basis functions, and F_{ij}^- is constructed from the solutions in the outer region such that it satisfies the boundary condition

$$\boldsymbol{F}^- \sim (\pi k)^{-1/2}(\sin\theta + \cos\theta\, \boldsymbol{K})(1 + \mathrm{i}\boldsymbol{K})^{-1} \tag{21}$$

corresponding to a Coulomb modified plane wave plus an ingoing spherical wave.

3. Calculations

The calculation of the photoionization cross sections in Li has been carried out in the low-energy region up to the 1s2l thresholds with emphasis given to a detailed investigation of

resonance structures. In order to explore the convergence of the close-coupling expansion we have used two approximations: a five-state close-coupling approximation, 5CC, which includes the target states $1s^2$, 1s2s ^{1,3}S and 1s2p ^{1,3}P, and an 11-state approximation, 11CC, which includes additionally 1s3l $^{1,3}L$ states. Besides, in each case results have been obtained with and without inclusion of correlation functions to explore the importance of the short-range correlation. In this section, we describe the intrinsic features of the present method and some computational details.

3.1. Calculation of the initial state

All bound states in this work were calculated with the finite-difference multiconfiguration Hartree–Fock (MCHF) atomic structure package (Froese Fischer *et al* 1997). For the initial $1s^22s$ state we use a straightforward *active-set* approach, generating all possible configuration state functions (CSFs) from a given set of orbitals called the active set. The results are given in table 1. $n_{\max}$ defines the active set of orbitals (all orbitals with $n \leqslant n_{\max}$ are included). The results should be compared with the 'exact' energy of $-7.478\,060$ au, obtained by McKenzie and Drake (1991) and Chung (1991). Because the computational effort for exploring the resonance photoionization at many energy points depends crucially on the number of CSFs, and because we are not interested in extremely accurate calculations, but rather only in obtaining an estimate of the efficiency of the present approach, in the final calculations we include only CSFs with expansion coefficients greater than 0.0001. The corresponding final energy is also presented in table 1.

Table 1. Resulting energies (in atomic units) from MCHF calculations for the ground state of Li.

CSFs included	Number of CSFs	Energy
$1s^22s$	1	$-7.432\,727$
$n \leqslant 2$	4	$-7.454\,565$
$n \leqslant 3$	27	$-7.473\,126$
$n \leqslant 4$	110	$-7.476\,125$
$n \leqslant 5$	348	$-7.477\,071$
$n \leqslant 6$	866	$-7.477\,467$
$c < 0.0001$	110	$-7.477\,064$[a]
		$-7.478\,060$[b]

[a] Approximation used.
[b] Exact value (McKenzie and Drake 1991).

3.2. Calculation of target states

The two-electron target state wavefunctions for Li^+ have been obtained from a set of separate independent MCHF calculations that lead to the non-orthogonal one-electron orbitals for different states but give the minimum number of CSFs required to achieve the same level of accuracy. For the same reason, instead of the active-set approach we use reduced 'natural' expansions (Froese Fischer *et al* 1997), with inclusion of one pair of orbitals at a time.

The resulting configuration expansions and energies for target states are given in tables 2–4 and are compared with 'exact' energies by Accad *et al* (1971). The 'final results' in the tables were obtained by additional overall re-optimization of one-electron functions. The orbitals in the first dominant configuration are the 'spectroscopic' ones, all others are to be considered as 'correlated'. An additional complication here is that the 'natural' expansion approach leads

Table 2. Resulting energies (in atomic units) from MCHF calculations for the $1s^2$ and 1s2s ^{1}S states.

CSFs included	$1s^2\ ^1S$	1s2s ^{1}S
1s2s		−5.099 223
$1s^2$	−7.236 415	−5.036 224
$+2p^2$ (+ $2s^2$ for ground state)	−7.272 608	−5.037 163
$+3s^2$, $3p^2$, $3d^2$	−7.277 363	−5.040 196
$+4s^2$, $4p^2$, $4d^2$, $4f^2$	−7.278 591	−5.040 574
$+5s^2$, $5p^2$, $5d^2$, $5f^2$, $5g^2$	−7.279 034	−5.040 663
	−7.279 358[a]	−5.040 800[a]
	−7.279 913[b]	−5.040 877[b]

[a] Final result.
[b] Exact value (Accad *et al* 1971).

Table 3. Resulting energies (in atomic units) from MCHF calculations for the 1s2s ^{3}S, 1s2p ^{3}P and 1s2p ^{1}P states.

^{3}S		^{3}P		^{1}P
1s2s	−5.109 358	$1s2p_1$	−5.024 669	−4.990 107
+3s4s	−5.109 380	$+2s3p_1$	−5.026 253	−4.990 231
+2p3p	−5.110 624	$+2p_23d_2$	−5.027 425	−4.992 727
+3s4d	−5.110 698	$+3p_24d_2$	−5.027 516	−4.992 809
+4f5f	−5.110 708	$+3d_14f_1$	−5.027 580	−4.993 069
		$+4d_15f_1$	−5.027 592	−4.993 100
	−5.110 711[a]		−5.027 614[a]	−4.993 143[a]
	−5.110 727[b]		−5.027 716[b]	−4.993 351[b]

[a] Final result.
[b] Exact value (Accad *et al* 1971).

Table 4. Resulting energies (in atomic units) from MCHF calculations for the 1s3*l* states.

Term	CSFs included	Energy	Exact[a]
^{3}S	1s3s, 2p3p	−4.752 061	−4.752 076
^{1}S	1s3s, 1s2s, $1s^2$, $2l^2$, $3l^2$, $4l^2$	−4.733 706	−4.733 756
^{3}P	$1s3p_1$, $2s4p_1$, $2p_23d_2$, $3d_14f_1$	−4.730 405	−4.730 460
^{1}P	$1s3p_1$, $2s4p_1$, $2p_23d_2$, $3d_14f_1$	−4.720 132	−4.720 207
^{3}D	1s3d, $2p_13p_1$, $2p_24f$	−4.722 348	
^{1}D	1s3d, $2p_13p_1$, $2p_24f$	−4.722 368	

[a] Exact value (Accad *et al* 1971).

to non-orthogonal orbitals even within a single state (see, for example, the ^{1,3}P expansions in table 3, where additional subscripts on orbitals indicate the different non-orthogonal sets), while the resulting configuration expansions are more compact. The slowest convergence is observed for the ^{1}S term, with a maximum error in energy of 15 meV for the $1s^2$ ground state. For all other target states, the energy accuracy is estimated to be in the range of 1–5 meV. We can conclude that the separate MCHF calculations give rise to accurate results with a minimum number of CSFs. In total, we use only 85 CSFs for all 11 target states, at the price of a large number of different one-electron orbitals, namely 103 different one-electron orbitals in the present calculation. However, increasing the number of one-electron functions does not complicate the calculations, because the time-consuming computations and the required memory is defined primarily by the number of CSFs.

Table 5. Comparison of oscillator strengths between target states.

	Present results		
Transition	l-form	v-form	Exact values[a]
$1s^2\ ^1S–1s2p\ ^1P$	0.455	0.454	0.457
$1s^2\ ^1S–1s3p\ ^1P$	0.110	0.110	0.110
$1s2s\ ^1S–1s2p\ ^1P$	0.214	0.217	0.213
$1s2s\ ^1S–1s3p\ ^1P$	0.256	0.257	0.257
$1s2p\ ^1P–1s3s\ ^1S$	0.032	0.032	0.031
$1s3s\ ^1S–1s3p\ ^1P$	0.364	0.375	0.362
$1s2s\ ^3S–1s2p\ ^3P$	0.308	0.306	0.308
$1s2s\ ^3S–1s3p\ ^3P$	0.187	0.187	0.187
$1s2p\ ^3P–1s3s\ ^3S$	0.039	0.039	0.039
$1s3s\ ^3S–1s3p\ ^3P$	0.514	0.511	0.513
$1s2p\ ^1P–1s3d\ ^1D$	0.711	0.712	
$1s3d\ ^1D–1s3p\ ^1P$	0.015	0.010	
$1s2p\ ^3P–1s3d\ ^3D$	0.624	0.623	
$1s3p\ ^3P–1s3d\ ^3D$	0.091	0.094	

[a] Schiff *et al* (1971).

The additional standard check of accuracy of target wavefunctions is the accuracy of oscillator strengths for transitions between target states and the agreement of length and velocity forms. These data are presented in table 5 as compared with the accurate results by Schiff *et al* (1971) obtained on the basis of Hylleraas-type functions. Very close agreement between length and velocity forms and with the other accurate results indicates that the target wavefunctions include the main part of the correlation. The above-indicated small difference in target energies, which can affect the position of autoionizing resonances, can be removed by using in the final stage of the calculations of the photoionization cross sections the exact or experimental energies for the initial and target states.

3.3. Choice of correlation functions

Because we do not use any orthogonal constraints on the continuum wavefunctions, the present close-coupling equations contain all possible resonance states only in the form of closed channels. Consider, for example, the lowest autoionizing state $1s2s2p\ ^2P$. For this state, the five-state approximation contains all CSFs of the form $1s^2np$, $1s2sn$p, $1s2pn$s, $1s2pn$d and some additional CSFs with three excited electrons due to configuration mixing in the target wavefunctions. The correlation orbital in the target wavefunctions, however, were optimized to describe correlation between the 1s and outer electrons, and it can be expected that the five-state expansion does not describe the correlation between two outer electrons on the same level. The 11-state approximation contains additionally the configurations $1s3lnl'$ but it is well known that the convergence of the close-coupling expansion is rather slow. Therefore, we also include additional correlation functions in our close-coupling expansion, in order to saturate the function space for a better description of the correlation between the outer electrons.

Using the non-orthogonal technique for the calculation of the matrix elements, we are not restricted to any artificial conditions on the choice of the correlation functions. For rapid convergence it is desirable that the correlation functions do not overlap considerably with that part of configuration space which is already included in the close-coupling expansion. Therefore, we use the following algorithm for generating the correlation functions. First we

generate the 1s, 2s, 2p orbitals from the average-term calculations for the 1s2s and 1s2p states. These orbitals are close to the spectroscopic orbitals used for the description of the target states, described above. Then we generate from these orbitals all possible CSFs for the ^{2}P term. Then we add the set of correlation orbitals 6s, 6p, 6d, 6f, 6g, 6h (here the principal quantum number has no important meaning and only represents an index) and form the set of all possible correlation CSFs 1s6l6l' and 6l6l'6l'' ^{2}P. Having in mind the correlation in the lowest autoionizing states, the correlation radial functions are obtained from the optimization of the lowest 1s2s2p ^{2}P state in the MCHF mode. Here the correlation orbitals 6l are orthogonal to the 1s, 2s and 2p orbitals, so they are approximately orthogonal to the spectroscopic orbitals used for construction of target states and the set of correlation CSFs 1s6l6l' and 6l6l'6l'' ^{2}P span a functional space which is approximately complementary to the bound channels of the close-coupling expansion. In final calculations, only those correlation functions which contribute to the trial 1s2s2p ^{2}P expansion with a coefficient greater than 0.01 have been included (25 correlation configurations in all).

3.4. Choice of grid

All further calculations were carried on the B-spline basis, and all target orbitals were expanded in the spline basis as

$$P_a(r) = \sum_i a_i B_i(r). \tag{22}$$

An important decision here is the selection of the grid. With splines, we can create any composite grid if needed since too rich a grid can lead to a rapid saturation of the computational resources. The existing experience shows that the most appropriate choice is a logarithmic grid that reflects the exponential behaviour of the atomic orbitals. On the other hand, in the continuum calculations, the wavelength of the scattering particle cannot be smaller than the grid step otherwise the B-spline basis hardly describes the oscillating behaviour of the wavefunction. In results, to define the grid, we introduce four different parameters: the step size in the origin, $h = 2^{-m}$, where m is an integer, the maximum step size $h_{\max}$, the maximum range $r_{\max}$ and the order of splines k_s. Let Z be the nuclear charge of the atom. The grid points are now defined through the array t_i, such that

$$\begin{aligned}
&t_i = 0 && \text{for} \quad i = 1, \ldots, k_s \\
&t_{i+1} = t_i + h && \text{for} \quad i = k_s, \ldots, k_s + m \\
&t_{i+1} = t_i(1 + h) && \text{for} \quad 1 < t_{i+1} - t_i < h_{\max} \\
&t_{i+1} = t_i + h_{\max} && \text{for} \quad t_i/Z < t_{\max} \\
&r_i = t_i/Z && \forall i.
\end{aligned} \tag{23}$$

In the present calculations we have used the following parameters:

$$Zh = 0.125 \qquad Zh_{\max} = 1 \qquad r_{\max} = 25 \qquad k_s = 8$$

which leads to the number of splines $N_s = 105$. $r_{\max}$ was chosen from the condition that for all bound radial functions $|P(r_{\max})| < 10^{-5}$, and this value coincides with R-matrix boundary, a.

3.5. Calculation of the interaction matrix

From a computational point of view, the main and only difference between the standard R-matrix approach and previous B-spline applications relates to the calculation of the interaction matrix (10). The eigenproblem (10) in the B-spline basis leads to a generalized eigenvalue problem, of the form

$$\boldsymbol{H}\boldsymbol{c} = E\boldsymbol{S}\boldsymbol{c}. \tag{24}$$

The solution vector, $\boldsymbol{c}$, can be written as

$$\boldsymbol{c} = [\boldsymbol{a}_1, \ldots, \boldsymbol{a}_{N_c}, \boldsymbol{b}]^T \tag{25}$$

where each $\boldsymbol{a}_i$ is a column vector of B-spline coefficients for given channel functions $\bar{\Phi}_i^{\Gamma}$

$$\boldsymbol{a}_i = [a_{1i}, a_{2i}, \ldots, a_{N_s i}]^T \tag{26}$$

and $\boldsymbol{b}$ is the column vector of the correlation function coefficients

$$\boldsymbol{b}_j = [b_1, b_2, \ldots, b_{N_p}]^T \tag{27}$$

where N_c is the number of channels, N_p is the number of correlation functions. Schematically, the interaction matrix $\boldsymbol{H}$ has the following form:

$$\begin{pmatrix} H(11) & H(12) & \cdots & H(1N_c) & h(1p) \\ H(21) & H(22) & \cdots & H(2N_c) & h(2p) \\ \vdots & \vdots & \ddots & \vdots & \vdots \\ H(N_c1) & H(N_c2) & \cdots & H(N_cN_c) & h(N_cp) \\ h(1p)^T & h(2p)^T & \cdots & h(N_cp)^T & h(pp) \end{pmatrix} \tag{28}$$

where $h(pp)$ is an $N_p \times N_p$ matrix and comes from the bound–bound interaction, $h(ip)$ are the $N_s \times N_p$ matrices, representing the interaction between the ith channel and bound states, $H(ij)$ are the $N_s \times N_s$ matrices for channel–channel interaction. $\boldsymbol{S}$ is the overlap matrix which in the case of the usual orthogonal conditions on scattering orbitals reduces to the matrix, consisting of diagonal blocks of the banded overlap matrix $\boldsymbol{B}$

$$B_{ij} = \langle B_i | B_j \rangle \tag{29}$$

one for each channel, but in the more general case of non-orthogonal orbitals has a more complicated structure (see table 6).

The most challenging question of the present algorithm is the effective way of determining the needed matrix elements in the basis of non-orthogonal orbitals. For this task we use the new program, BREIT_NO (Zatsarinny and Froese Fischer 1999), which performs the angular integrations necessary for expressing the matrix elements of the Breit–Pauli Hamiltonian as a linear combination of radial integrals. Any amount of non-orthogonality between the orbitals may be present leading to overlap factors in the matrix elements. The calculations follow the method based on the representation of configuration wavefunctions through the Slater determinants (Zatsarinny 1996). The program also allows one to reuse angular data obtained previously through the creation of a data bank for angular coefficients. This program is central in the computational implementation of the present approach.

Each individual matrix element in (28) is expressed by the program BREIT_NO in the form

$$\sum c_i L(a, b) \times D(\{nl\}; \{n'l'\}) + \sum c_i R^{\lambda}(a, b; c, d) \times D(\{nl\}; \{n'l'\}) \tag{30}$$

Table 6. Contribution of different terms (without indication of angular coefficients) in the interaction matrix. Symbols a, b, c, d stand for the bound orbitals, the symbol k_i indicates the continuum orbital in channel i.

Term	Contribution	Remarks
Channel–channel interaction		
$R^\lambda(k_i, a; k_j, b)$	$R^\lambda(\cdot a \cdot b)$	Banded matrix, direct interaction
$R^\lambda(k_i, a; b, k_j)$	$R^\lambda(\cdot\cdot ab)$	Full matrix, exchange interaction
$R^\lambda(k_i, a; b, c)\langle d\|k_j\rangle$	$R^\lambda(\cdot abc) \cdot B(\cdot d)$	Full matrix, contribution due to non-orthogonality
$\langle k_i\|a\rangle\langle b\|k_j\rangle R^\lambda$ (or L)	$B(\cdot a) \cdot B(\cdot b) * R^\lambda$ (or L)	Full matrix, contribution due to non-orthogonality
$\langle k_i\|k_j\rangle R^\lambda$ (or L)	$B(\cdot\cdot) * E_i$	Banded matrix, only for $i = j$
$L(k_i, k_j)$	$L(\cdot\cdot)$	Banded matrix, only for $i = j$
$L(k_i, a)\langle b\|k_j\rangle$	$L(\cdot a) \cdot B(\cdot b)$	Full matrix, contribution due to non-orthogonality
$\langle k_i\|k_j\rangle$	$B(\cdot\cdot)$	Banded matrix, only for $i = j$, contribution to overlap matrix
$\langle k_i\|a\rangle\langle b\|k_j\rangle$	$B(\cdot a) \cdot B(\cdot b)$	Full matrix, contribution to overlap matrix due to non-orthogonality
Channel–bound interaction		
$R^\lambda(k_i, a; b, c)$	$R^\lambda(\cdot abc)$	Vector
$L(k_i, a)$	$L(\cdot a)$	Vector
$\langle k_i\|a\rangle R^\lambda$ (or L)	$B(\cdot a) * R^\lambda$ (or L)	Vector, contribution due to non-orthogonality
$\langle k_i\|a\rangle$	$B(\cdot a)$	Vector, contribution to overlap matrix
Bound–bound interaction		
$R^\lambda(a, b; c, d)$		Scalar
$L(a, b)$		Scalar
c		Scalar, contribution to overlap matrix

where c_i are the numerical coefficients which depend only on the angular symmetry of the involved CSFs, L denotes one-electron integrals, R^λ are Slater integrals and $D(\{nl\}, \{n'l'\})$ is the overlap factor which depends only on the orthogonality of radial orbitals used for the construction of basis CSFs. In general, the overlap factor is the multiplier of determinants of matrices consisting of one-electron overlaps

$$\begin{vmatrix} \langle n_1 l|n'_1 l\rangle & \langle n_1 l|n'_2 l\rangle & \dots & \langle n_1 l|n'_q l\rangle \\ \langle n_2 l|n'_1 l\rangle & \langle n_2 l|n'_2 l\rangle & \dots & \langle n_2 l|n'_q l\rangle \\ \dots & \dots & \dots & \dots \\ \langle n_q l|n'_1 l\rangle & \langle n_q l|n'_2 l\rangle & \dots & \langle n_q l|n'_q l\rangle \end{vmatrix}. \tag{31}$$

The scattering orbitals can appear in the radial integrals L and R^λ, and also in the determinant factors. To derive the final expression for the matrix elements in the B-spline basis, let us first simplify the overlap factors (31) by expanding them over those rows which contain one-electron overlaps with the scattering orbitals. At most, there can be two such rows. The residual

overlap determinant depends only on the known bound orbitals and they can be calculated in the standard manner. It is convenient to redefine the coefficients c_i by multiplying them by these residual overlap factors. As a result, the initial overlap factor $D(\{nl\}, \{n'l'\})$ in expression (30) is reduced to the one- or two-electron overlaps of the form

$$\langle kl|nl\rangle \quad \langle kl|k'l\rangle \quad \text{or} \quad \langle kl|nl\rangle\langle n'l'|k'l'\rangle \tag{32}$$

where $|kl\rangle$ denotes the radial function of the continuum orbital in the inner region

$$u_{kl}(r) = \sum_i a_i B_i(r). \tag{33}$$

Each term in expression (30) gives rise to some matrix in the spline basis. To elucidate the structure of these matrices, let us introduce, in addition to the overlap B-matrix defined in equation (29), the following $N_s \times N_s$ matrices with elements

$$\begin{aligned} L(\cdot\cdot)_{ij} &= \langle B_i|\frac{\mathrm{d}^2}{\mathrm{d}r^2} - \frac{l(l+1)}{r^2} + \frac{2Z}{r}|B_j\rangle \\ R^\lambda(\cdot\cdot ab)_{ij} &= \sum_{i',j'=1}^{N} a_{i'}b_{j'}R^\lambda(ij;i'j') \\ R^\lambda(\cdot a\cdot b)_{ij} &= \sum_{i',j'=1}^{N} a_{i'}b_{j'}R^\lambda(ii';jj') \end{aligned} \tag{34}$$

where

$$R^\lambda(ij,i'j') = \langle B_i(r_1)B_j(r_2)|U_{12}^\lambda|B_{i'}(r_1)B_{j'}(r_2)\rangle \tag{35}$$

U_{12}^λ is the radial part of the λth term in the multipole expansion of $1/r_{12}$, and $a_{i'}$, $b_{j'}$ are the expansion coefficients in a spline basis for bound orbitals $P_a(r)$, $P_b(r)$ (see equation (22)). In effect, the four-dimensional array, $R^\lambda(ij;i'j')$, represents the Slater integral in the spline basis. The integrals are zero if either $|i - i'| \geqslant k_s$ or $|j - j'| \geqslant k_s$. Methods for computing these quantities, which depend only on the basis, have been described elsewhere (Froese Fischer *et al* 1992). To describe the channel–bound interaction, let us introduce the following vectors with elements:

$$B(\cdot a)_i = \sum_j^{N_s} a_j B_{ij} \tag{36}$$

$$L(\cdot a)_i = \sum_{j=1}^{N_s} a_j L_{ij} \tag{37}$$

$$R^\lambda(\cdot abc)_i = \sum_{j=1}^{N_s} c_j R^\lambda(\cdot\cdot ab)_{ij}. \tag{38}$$

With this notation, table 6 represents the contribution of the different terms from the energy expression (30), which usually produces the angular integration codes, to the interaction matrix (28), along with an indication of its structure. Table 6 also indicates the contribution to the total overlap matrix arising from the matrix element in the right-hand side of equation (10). Note that we assume that target wavefunctions form an orthogonal set and diagonalize the target Hamiltonian. Hence, of all matrix elements containing $\langle kl|k'l\rangle$, only diagonal ones, with $k = k'$, contribute to the interaction matrix. The same concerns the matrix elements with $L(kl, k'l)$.

3.6. Calculation of dipole matrix elements

The reduced matrix elements between the initial state and R-matrix basis functions, $(\Psi_k \| D \| \Psi_0)$, which are needed for evaluation of photoionization cross sections, have the following form, which is non-trivial in the general case of non-orthogonal orbitals,

$$\sum c_i \langle P^{(k)}_{kl',n'l'} | \boldsymbol{d} | P^{(0)}_{nl} \rangle \times D(\{kl', n'l'\}; \{nl\}) \tag{39}$$

where c_i is the angular coefficient, $\boldsymbol{d}$ is the dipole operator in the length or velocity form, $P^{(0)}(r)$ and $P^{(k)}(r)$ are the radial orbital in the initial and continuum state, respectively. $D(\{nl\}, \{n'l'\})$ is the overlap factor of the form (31) which depends only on the orthogonal conditions between radial orbitals used for the construction of basis CSFs for initial and final states. Expression (39) includes in a natural way the relaxation effects which can occur during the photoionization process. The angular integration, necessary to obtain coefficients c_i, was carried out in the present calculations according to the algorithm suggested by Zatsarinny (1996). The advantage of using a non-orthogonal basis for the initial and final states is that these states can be obtained from independent calculations, which in turn considerably extends the range of different optimization procedures which can be used. Note also, that the evaluation of numerical dipole integrals in (39) for the length form was done by a straightforward integration using Gaussian quadrature. For the velocity form, as well as for L integrals (34), advantage is taken of the fact that the B-spline basis functions can be differentiated analytically.

3.7. Extraction of resonance positions and widths

For comparison with experiment and other theories, we need to deduce a position and total and partial widths for each resonance. A number of programs have been developed for analysing the resonances in atomic and molecular physics. Most of them use the numerical fitting procedures based on the energy variation of calculated scattering parameters (e.g. the reactance matrix, K, or its eigenphases, δ, or cross sections, σ, or others) near the isolated resonance. For example, the two widely used published programs, RESFIT (Bartschat and Burke 1986) and RESON (Tennyson and Noble 1984), both make use of energy derivatives, which are calculated numerically from the K-matrix tabulated on a predetermined energy mesh. Another method, programmed in the TIMEDEL package (Stibbe and Tennyson 1998), is the 'time-delay' method where the S-matrix is evaluated just below and just above a resonance to find the time-delay matrix $-\mathrm{i}\hbar \boldsymbol{S}\, \mathrm{d}\boldsymbol{S}/\mathrm{d}E$ numerically, the largest eigenvalue of which is analysed for the resonance parameters. All the above procedures are difficult to automate on a computer to find a series of resonances, and typically involve working interactively, because the fitting accuracy depends on evaluating the K-matrix at enough energies around the resonances. Graphical user interfaces have been developed for these interactive procedures (e.g. Busby *et al* 1998).

In connection with the present R-matrix approach, the QB program by Quigley *et al* (1998) seems to be most effective for analysis of resonances. It is based on the eigenphase fitting procedure, but uses R-matrix theory to determine the energy variation of the eigenphase analytically rather than numerically. The QB method defines matrices $\boldsymbol{Q}$ and $\boldsymbol{B}$ in terms of asymptotic solutions, the R-matrix and energy derivatives, such that $\mathrm{d}\boldsymbol{K}/\mathrm{d}E = \boldsymbol{B}^{-1}\boldsymbol{Q}$, from which eigenphase gradients of the $\boldsymbol{K}$-matrix can be obtained. Resonance positions are defined at the point of the maximum gradients; resonant widths are related to the inverse of the eigenphase gradient. The required energy derivative of the R-matrix is defined analytically by differentiating equation (13). The method allows one to fully automate the procedure

of detecting resonances with a minimum number of calculations in the outer region for different energies. It also processes the overlapping resonances well. The QB method therefore requires only the data to construct the R-matrix in equation (13) for a given energy, together with the external region solutions and their derivatives at $r = a$. All these data are generated in the present algorithms, and we can use the QB method without additional calculations.

In order to remove the uncertainties in the resonance position due to residual errors in the target energies, we use the experimental energies of target states for calculations of outer region solutions, photoionization cross sections and in the QB analysis of resonances. Here the target energies define only the kinematic properties of the scattering electron and scarcely effect its interaction with target electrons. On the other hand, in the inner region, the target energies enter into the interaction matrix through the terms $B(\cdot\cdot) \times E_i$, and due to multiplication with B-spline overlaps the small changes in E_i can destroy the consistency in the generalized eigenvalue problem (10) and give rise to large errors both in the position and width of the resonances. For this reason, we use only theoretical energies for the calculation of the interaction matrix in the inner region.

It should also be noted that in contrast to the direct method of solving the close-coupling equations in the B-spline basis (see equations (3) and (4), and references after them), the present R-matrix method allows us to obtained parameters for all Rydberg series of resonances without increasing the boundary radius $r_{\max} = a$, at a price of additionally solving the scattering equation in the outer region which is a much easier task. It is very important from a computational point of view because the increase of the boundary radius leads to a very large number of B-splines, and, consequently, to a very large dimension of the interaction matrix.

4. Results and discussion

A large amount of experimental and theoretical data exist for Li photoionization. Experimentally, Hudson and Carter (1967) measured 2s photoionization of lithium over photon energies from threshold to about 22 eV using a photoelectron technique. Ferrett *et al* (1987) have performed measurements on 1s photoionization of lithium corresponding to the 1s2s ^{1}S and ^{3}S ionic states. Langer *et al* (1991) also measured the partial cross sections and angular distribution asymmetry parameters of Li 1s photoionization using synchrotron radiation. On the theoretical side, several calculations on photoionization of lithium using various techniques have appeared in the literature (Larkins *et al* (1981), Kupliauskene (1996), relaxed Hartree–Fock model; Armen *et al* (1990), Armen and Larkins (1991), configuration-interaction method; Saha and Lin (1997), MCHF method for continuum wavefunctions; Lisini *et al* (1990), 11-state R-matrix calculations). As a result, the total and partial photoionization cross sections and relevant shake-up processes in Li are well understood.

The resonance structure in photoionization has received much less attention. The first high-resolution spectrum of core-excited lithium is reported by Ederer *et al* (1970) using synchrotron radiation. They defined energy positions of the 1s2s(^{3}S)np ^{2}P^o, 1s2p(^{1}P)ns ^{2}P^o and 1s2p(^{1}P)nd ^{2}P^o states. Recently, a very impressive high-resolution photoion spectrum of Li has been obtained in the synchrotron-related experiment by Kiernan *et al* (1996). The resonance positions and other properties in the resonance photoionization of atomic lithium in the region of the first two inner-shell thresholds were measured. They also reported a 19-state R-matrix calculation which showed good agreement with the measurements, though specific details of the calculation such as resonance positions, widths and profile were not reported.

Instead, they analysed and identified their spectra mainly using a quantum defect method. This precise experiment has stimulated two further large-scale theoretical investigations. Chung (1997a) using a saddle-point complex-rotation method obtained excellent, almost point-to-point agreement with the measurements in the inelastic energy region that allowed him to give detailed identification on resonance features, with several earlier identifications being reassigned. Unfortunately, the theoretical results were only presented in a graphical way that further complicated comparison with other data. Then, Chung (1997b) also carried out a detailed consideration of the photoionization of lithium below the 1s2s ^{3}S threshold and presented the resonance energy, width and photoionization cross section for the lowest 14 resonances. Another large-scale calculation of the Li photoionization has been carried out by Vo Ky *et al* (1998) in the 19-state *R*-matrix approximation. They repeated the results of the 11-state *R*-matrix calculations by Lisini *et al* (1990) concerning the shake-up processes with the 1s2*l* final ionic states. It indicates the convergence of close coupling in this energy region. Some improvement of partial cross section has been obtained in the region of the 1s3*l* final ionic states. They also suggest new assignment of the resonance features using the new eigenchannel treatment of *R*-matrix theory (Li *et al* 1997) but this assignment differs greatly from the assignment given by Kiernan *et al* (1996) and Chung (1997a).

Below we present results of calculations of the resonance photoionization of Li in the region of the 1s2*l* final states. The calculations were performed in the 11-state approximation with inclusion of short-range correlation functions. We will not present the total and partial cross sections at energies outside the resonance region, because they are in very close agreement with the above-mentioned results and they do not lead to new physical conclusions. We will concentrate on the identification of resonances and on the determination of their parameters such as energies and widths. Namely, these are the quantities most sensitive to the electron–electron correlation and to the accuracy of the representation of the target wavefunctions. We believe that our approach is more appropriate in this respect.

4.1. Resonances below the 1s2s ^{3}S excitation threshold

The energies and widths for the ^{2}P^o resonances in this energy region are presented in table 7 compared with experimental data and recent theoretical results by Chung (1997b) and Vo Ky *et al* (1998). The photoionization spectrum here has the simple pattern of a series of well separated narrow resonances, 1s2s(^{3}S)*n*p, perturbed by the 1s2s(^{1}S)3p state. Our energy positions agree well with the experimental values from photoionization measurements and with the saddle-point complex-rotation calculation by Chung (1997b). The somewhat larger error for energy positions of the first two resonances 1s(2s2p ^{1,3}P) may be attributed to the incomplete inclusion of the short-range correlation (see below the discussion about convergence of the present close-coupling expansion in section 4.5). As is seen from table 7, the present 11-state *R*-matrix calculations considerably improve the 19-state *R*-matrix results of Vo Ky *et al* (1998). It is due to a much more accurate description of target states in the present approach and due to the additional inclusion of correlation wavefunctions for the description of short-range correlation.

Our autoionizing widths also agree very well with values obtained by Chung (1997b) including the drastic influence of the 1s2s(^{1}S)3p perturber. It is well known that the Auger width of a Rydberg series should be decreasing monotonically as *n* increases. We see from table 7 that the width decreases quickly from the two lowest resonances to 1s2s(^{3}S)3p and 1s2s(^{3}S)4p, as expected. However, the widths for 1s2s(^{3}S)4p and 1s2s(^{3}S)5p are equal, and

Table 7. Energies and widths of autoionization states in Li below the 1s2s ^{3}S threshold (64.413 eV).

	Energies (eV)						Widths (meV)	
State	Expt[a]	Expt[b]	Expt[c]	Calc.[d]	Calc.[e]	Calc.[f]	Calc.[e]	Calc.[f]
1s(2s2p)^{3}P		58.910	58.909		58.910	58.916	3.33	3.48
1s(2s2p)^{1}P		60.396	60.392		60.398	60.409	9.56	9.54
1s2s(^{3}S)3p	62.422	62.419	62.417	62.386	62.417	62.423	0.203	0.196
1s2s(^{3}S)4p	63.353	63.356	63.358	63.329	63.351	63.353	0.044	0.041
1s2s(^{3}S)5p	63.752	63.753	63.755	63.745	63.750	63.752	0.044	0.041
1s2s(^{3}S)6p	63.951	63.951	63.956	63.918	63.950	63.951	0.140	0.131
1s2s(^{1}S)3p	64.050	64.046	64.052	64.029	64.050	64.051	0.391	0.352
1s2s(^{3}S)7p	64.121	64.121	64.118	64.075	64.119	64.121	0.255	0.230
1s2s(^{3}S)8p	64.183	64.184	64.181	64.165	64.182	64.184	0.107	0.101
1s2s(^{3}S)9p	64.231	64.232	64.228	64.221	64.230	64.232	0.061	0.058
1s2s(^{3}S)10p	64.266	64.260	64.258	64.260	64.265	64.267	0.041	0.040
1s2s(^{3}S)11p	64.292			64.288	64.293	64.293	0.033	0.030
1s2s(^{3}S)12p	64.311			64.303	64.313	64.312	0.027	0.023

[a] Ederer *et al* (1970), photoionization measurements (±0.006 eV).
[b] Cantu *et al* (1977), photoionization measurements (±0.003 eV).
[c] Kiernan *et al* (1996), photoion spectra measurements (±0.010 eV).
[d] Vo Ky *et al* (1998), 19-state *R*-matrix calculations.
[e] Chung (1997), saddle-point complex-rotation method.
[f] Present work.

the width of the 1s2s(^{3}S)6p state is larger than that of 1s2s(^{3}S)5p by a factor of 3. This is because of the strong mixing of the 1s2s(^{3}S)*n*p states with the perturber, which has a much larger width itself. This change of widths from the usual pure Rydberg series also gives rise to the irregular intensity pattern observed in the experiment by Kiernan *et al* (1996) and fully explained by Chung (1997b).

The width of the lowest 1s(2s2p ^{3}P) state has been measured by Mannervik and Cederquist (1985) to be 2.6(1) meV and by Pedrotti (1987) to be 3.2(6) meV. The present result agrees with the latter result, where, however, a larger error bar is quoted.

It should be noted that the autoionizing widths are extremely sensitive to approximations used in the calculation, and can serve as a sensitive probe of the accuracy of approximation. In particular, it concerns the lowest autoionizing states and perturbers. The good agreement of our autoionizing widths with results of Chung (1997b) and a good agreement with experimental positions along the whole perturbed series reflects the high accuracy of the present approach.

4.2. Resonances in the 1s2s ^{3}S–1s2s ^{1}S energy region

The lithium spectrum between the 1s2s ^{3}S and 1s2p ^{3}P excitation thresholds is a classical example of a complex and highly irregular resonance spectrum. It is caused by the strong mixing in this energy region of the five resonance series, 1s2s(^{1}S)*n*p, 1s2p(^{3}P)*n*s, 1s2p(^{3}P)*n*d, 1s2p(^{1}P)*n*s and 1s2p(^{1}P)*n*d. A positive identification of the structure in this region needs detailed theoretical calculations and for a long time, since the first measurements by Ederer *et al* (1970), remained an open question.

The energies and widths for autoionizing states in this energy region are presented in table 8 along with results of recent experimental and theoretical studies. The corresponding photoionization spectrum is depicted in figures 1 and 2. To gain a better understanding of

Table 8. Energies and total and partial widths of autoionization states in Li below the 1s2s ^{1}S threshold (66.314 eV).

	Energies (eV)					Widths (meV)		
State	Expt[a]	Calc.[b]	Calc.[c]	Calc.[d]	Label[d]	Calc.[b]	%[b]	Calc.[c]
1s2p(^{3}P)3s	64.569	64.575	64.554	64.536	3d	113	91.5	105
1s2s(^{1}S)4p	∼65.2	65.152	65.121	64.806	3s	84.0	84.0	95
1s2p(^{3}P)3d	65.244	65.262	65.233	65.227	4d	19.5	99.4	9
1s2p(^{1}P)3s	65.289	65.301	65.282	65.282	3s′	2.82	88.1	2
1s2p(^{3}P)4s	65.535	65.570	65.551	65.625	4s	66.3	98.5	63
1s2s(^{1}S)5p	65.664	65.671		65.805	5p′	3.52	74.7	
1s2p(^{3}P)4d		65.861		65.878	5d	0.975	82.1	
1s2s(^{1}S)6p	65.874	65.873		65.941	6p′	6.63	92.5	
1s2s(^{1}S)7p	65.994	65.989		66.005	3d′	12.5	99.2	
1s2p(^{3}P)5s		66.018		66.035	5s	16.6	95.3	
1s2s(^{1}S)8p		66.075		66.074	7p′	0.154	18.7	
1s2s(^{1}S)9p		66.126		66.122	8p′	0.199	59.1	
1s2p(^{1}P)3d	66.379	66.146		66.155	6d	3.11	99.1	
1s2s(^{3}P)5d		66.163				1.46	92.2	
1s2s(^{1}S)10p		66.189		66.183	9p′	0.823	92.2	
1s2s(^{1}S)11p		66.206		66.196	10p′	0.125	97.6	
1s2s(^{1}S)12p		66.220		66.211	11p′	0.595	51.6	
1s2p(^{3}P)6s		66.231		66.225	12p′	1.08	95.1	
1s2s(^{1}S)13p		66.242		66.236	13p′	0.063	37.4	
1s2s(^{1}S)14p		66.251		66.250	6s	0.060	53.1	
1s2s(^{1}S)15p		66.258		66.255	14p′	0.107	74.4	
⋮								
1s2p(^{3}P)6d		66.306		66.302	7d	1.08	99.1	

[a] Kiernan *et al* (1996), photoion spectra measurements (±0.010).
[b] Present work. Column '%' gives the partial width in percentages for the 1s2s(^{3}S)ϵp decay channel.
[c] Quigly and Berrington (1996), 11-state *R*-matrix calculations.
[d] Vo Ky *et al* (1998), 19-state *R*-matrix calculations. Column 'Label' gives their classification of resonances.

the resonance identification, we additionally split the spectrum into two energy regions and made a detailed comparison with experiment by Kiernan *et al* (1996) in each region. The resonance positions and their assignments are marked in the figures for discussion purposes. Here we use the simplified labels for autoionizing states 1s2s(^{1,3}S)np and 1s2p(^{1,3}P)ns, nd as nl or nl', where a prime indicates the intermediate spin $S = 0$. Note that relative intensity measurements by Kiernan *et al* (1996) have been normalized to the absolute measurements by Mehlman *et al* (1978). The experimental points presented in figures 1–4 have been obtained from graphical representations of cross sections given by Kiernan *et al* (1996) and Chung (1997a), and therefore may contain some small additional shifts.

The spectrum presented in figure 1 contains eight resonances, the positions of which agree excellently with the experiment. Calculations also represent the intensities of resonance peaks well, and this representation may be expected to be better if the cross sections were convolved with an instrumental resolution. Our assignments for the resonances correlate well with the identification given by Chung (1997a). The main difficulty here is presented by the group of resonances in the range 65.1–65.3 eV. In order to clarify their classifications and to demonstrate the level of mixing of different resonance series in this region, table 9 represents the closed-

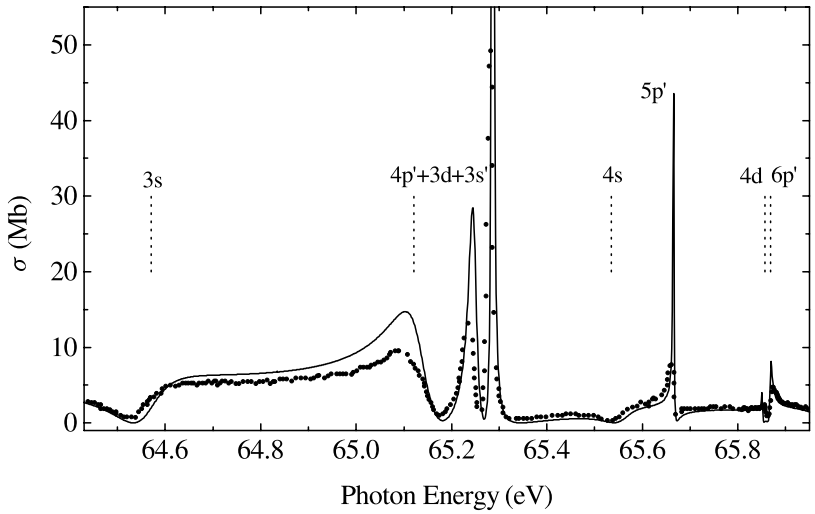

Figure 1. Photoionization cross section of Li below the 1s2s ^{1}S threshold, 64.4–65.9 eV region. Full curve, present theory; circles, experiment by Kiernan *et al* (1996).

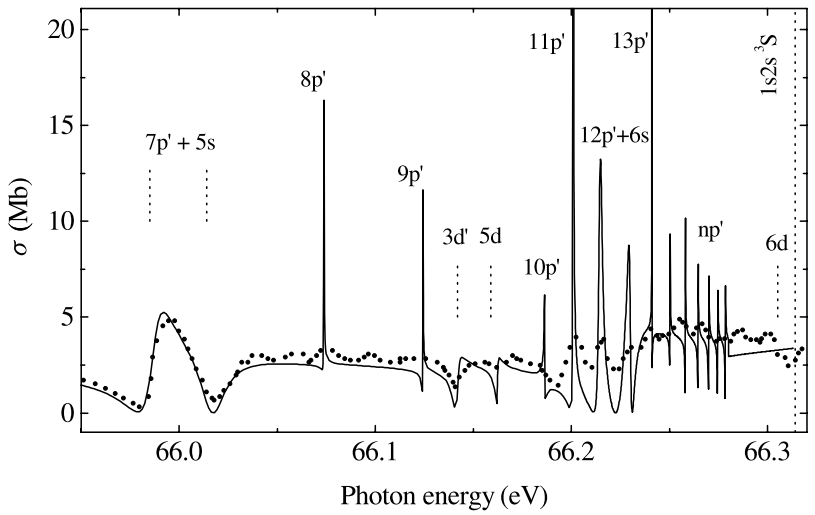

Figure 2. Photoionization cross section of Li below the 1s2s ^{1}S threshold, 65.9–66.32 eV region. Full curve, present theory; circles, experiment by Kiernan *et al* (1996).

channel mixing coefficients for the first ten resonances, obtained in the 11-state close-coupling approximation without any correlation functions. We see that the three resonances, 1s2s(^{1}S)4p, 1s2p(^{1}P)3s and 1s2p(^{3}P)3d, interact so strongly that it is not possible to define the dominant configuration. For this reason, these resonances are depicted in figure 1 as a sum of the above states, because the identification based on the independent particle model is not relevant for these low-lying states. It also concerns the resonances 1s2s(^{3}S)6p and 1s2p(^{3}P)4d, shown in figure 2. Note also the relatively small contribution of the closed channels connected with the 1s3*l* target states.

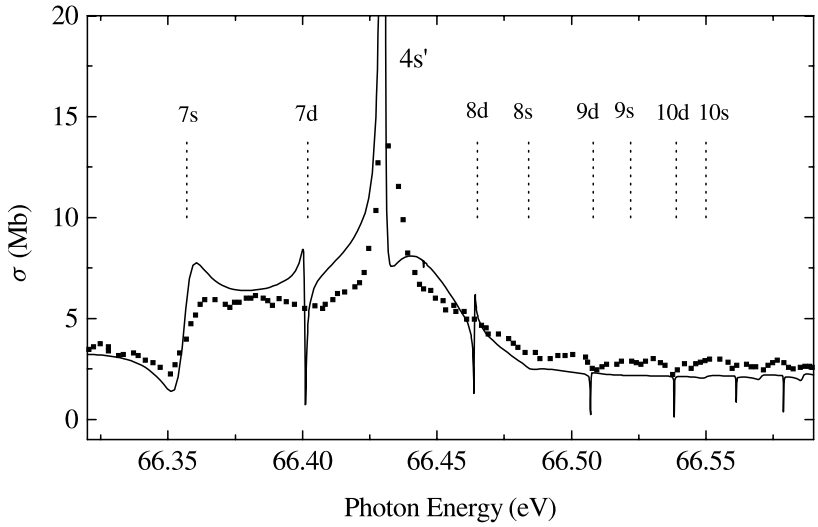

Figure 3. Photoionization cross section of Li below the 1s2p ^{3}P threshold. Full curve, present theory; circles, experiment by Kiernan *et al* (1996).

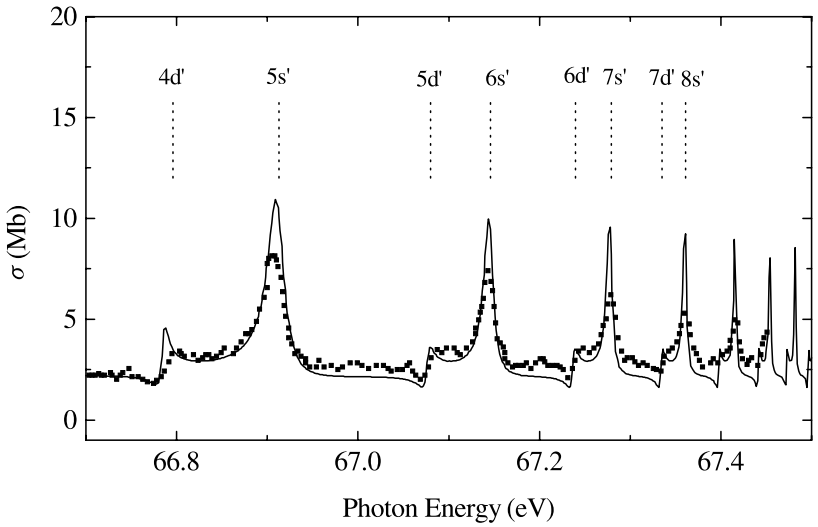

Figure 4. Photoionization cross section of Li below the 1s2p ^{1}P threshold. Full curve, present theory; circles, experiment by Kiernan *et al* (1996).

Our photoionization cross section is in close agreement with that obtained by Chung (1997a), but he did not present a list of energy positions and widths which can be used for a detailed comparison. The energy positions and widths for the first five resonances agree well with the results of Quigley and Berrington (1996) obtained in the 11-state *R*-matrix approximation. The width for the first resonance also agrees well with the experimental value of 0.1 eV by Kiernan *et al* (1996). Table 8 also gives information about partial widths (see the % column). They show that these resonances autoionize predominantly to the 1s2s ^{3}S excited state. This conclusion is opposite to the conclusion of Quigley and Berrington (1996), though

Table 9. Closed-channel mixing coefficients for the first ten autoionizing states above the 1s2s ^{3}S threshold, obtained in the 11-state close-coupling approximation.

No	Energy	1s2s(^{1}S)*n*p	1s2p(^{3}P)*n*s	1s2p(^{3}D)*n*d	1s2p(^{1}P)*n*s	1s2p(^{1}P)*n*d	1s3*lnl′*
1	64.575	14.9	69.7	1.8	4.2	0.5	8.9
2	65.152	45.5	4.3	0.8	40.1	0.8	7.9
3	65.262	16.4	5.7	56.6	17.3	1.5	2.5
4	65.301	32.4	0.5	54.6	10.8	1.2	0.5
5	65.570	23.9	60.6	1.3	9.6	0.2	3.4
6	65.671	74.9	20.0	0.1	2.0	1.2	1.8
7	65.861	5.3	10.5	67.1	12.2	0.2	4.3
8	65.873	75.8	9.2	10.1	2.0	1.2	1.7
9	65.989	45.8	43.1	0.9	6.3	1.4	2.5
10	66.018	42.4	51.6	0.3	0.7	2.8	2.2

we both used the same QB method and the same program QB by Quigley *et al* (1998) for the resonance analysis.

There is also rather good qualitative agreement with the photoionization cross section obtained by Vo Ky *et al* (1998) on the basis of a 19-state *R*-matrix calculation. At the same time table 8 shows significant differences with their classification of resonances. For identification of resonances they applied the new method proposed by Li *et al* (1997) for *R*-matrix calculations of photoionization. In this method, the wavefunctions in the outer region are calculated directly from the logarithmic derivatives of the solution at the boundary *R*-matrix and from the physical eigenchannel parameters (the quantum defect μ_α and the orthogonal transformation matrix $U_{i\alpha}$) in multichannel quantum defect theory. Such a unified theory between the *R*-matrix method and the quantum defect method was expected to be convenient for an analytic unified treatment of perturbed discrete Rydberg series, autoionizing states and their adjacent continuum, and also for a clear assignment of overlapping resonances. As noted by Quigley and Berrington (1996), this method seems to be very promising for the pure Coulomb problem. However, as the comparison with our results and the results of Chung (1997a) shows, this method gives rise to very different identifications for the many resonances in Li, and this identification is not fully justified.

Let us now consider the next energy region presented in figure 3. Kiernan *et al* (1996) identified the structure peaked at 65.994 eV to be the 1s2s(^{1}S)7p state, but this line has an unusual profile which is clearly different from the other members of this series. We found after Chung (1997a) that this structure is formed by the presence of two resonances, 1s2s(^{1}S)7p and 1s2p(^{3}P)5s, with quite even mixing, see table 9, levels 9 and 10. The energy positions for these states, 65.992 and 66.018 eV, given by Chung (1997a) agree very well with our results in table 8.

In the higher-energy part, between 66.1 and 66.2 eV, the resonances are not so clearly seen in the experiment. Nevertheless, we can also claim close agreement with measurements by Kiernan *et al* (1996), if the final experimental resolution were taken into account. To obtain the accurate resonance pattern in such a near-threshold region where many series overlap, it is necessary to use very accurate threshold energies for the overlapping series. The resonance pattern depicted in figure 2 was only obtained after introducing the experimental target energies for the solution in the asymptotic region (see section 3.7), though here the theoretical thresholds differ only by about 5 meV from the experimental results. It is clear that even a small relative shift of closely lying and strongly interacting resonances can lead to drastic changes in the overall resonance pattern. The energy region under consideration is just a typical example

Table 10. Energies and total and partial widths of autoionization states in Li below the 1s2p ^{1}P threshold (67.672 eV).

	Energy (eV)						Partial widths[a] (%)		
State	Calc.[a]	Calc.[b]		Calc.[c]		Width[a] (meV)	$1s^2kp$	$1s2s(^3S)kp$	$1s2s(^1S)kp$
1s2p(^{3}P)7s	66.357	66.359	7s	66.354	7s	9.69	21.5	57.9	20.6
1s2p(^{3}P)7d	66.402	66.404	7d	66.398	8d	0.92	0.8	83.8	15.4
1s2p(^{1}P)4s	66.433	66.434	4s′	66.429	8s	0.51	23.0	38.4	78.8
		66.447	8s	66.458	4s′				
1s2p(^{3}P)8d	66.465	66.466	8d	66.462	9d	0.49	1.5	20.4	78.1
1s2p(^{3}P)8s	66.484	66.488	9s	66.482	9s	7.58	1.0	61.8	37.2
1s2p(^{3}P)9d	66.508	66.510	9d	66.505	10d	0.34	0.7	60.0	39.3
1s2p(^{3}P)9s	66.524	66.541	10s	66.520	10s	5.38	2.5	64.7	32.8
1s2p(^{3}P)10d	66.539	66.560	10d	66.536	11d	0.27	0.7	65.4	33.9
1s2p(^{3}P)10s	66.550			66.545	11s	3.85	3.2	65.2	31.6
1s2p(^{3}P)11d	66.562			66.559	12d	0.22	0.6	67.1	32.3
1s2p(^{3}P)11s	66.570			66.566	12s	2.87	3.7	65.4	30.9
1s2p(^{3}P)12d	66.579			66.576	13d	0.18	0.6	67.6	31.8
1s2p(^{3}P)12s	66.586			66.584	13s	2.20	4.0	65.5	30.5

[a] Present work.
[b] Chung (1997), saddle-point complex-rotation method.
[c] Vo Ky *et al* (1998), 19-state *R*-matrix calculations.

in this respect. In this energy region we give somewhat different resonance assignments in comparison with Kiernan *et al* (1996) and Chung (1997a). This difference concerns mainly the assignment for the 1s2p(^{1}P)3d and 1s2p(^{3}P)5d states. In Kiernan *et al* (1996), the 1s2p(^{1}P)3d state is identified at 66.379 eV, above the 1s2s ^{1}S threshold. Chung (1997a) predicts the 1s2p(^{1}P)3d energy at 66.207 eV, whereas our position for this resonance is 66.146 eV. As is seen from figure 2, the nd resonances have a clearly different shape from the other series, and only interact weakly with the 1s2s(^{1}S)np series. The main perturber for the 1s2s(^{1}S)np series in this energy region is the 1s2p(^{3}P)6s state. This state interacts very strongly with the 1s2s(^{1}S)12p one, and, as is clearly seen in figure 2, considerably perturbs the series in the region from the 1s2s(^{1}S)10p up to 1s2s(^{1}S)14p states.

The program ASYPCK (Crees 1980), which we use in the present calculations to find asymptotic solutions in the outer region, has restrictions for near-threshold energies because it needs to perform numerical integrations to extremely high radii. It does not allow us to reproduce directly the photoionization cross sections for photon energies very close to excitation thresholds. Nevertheless, the QB-method program (Quigley and Berrington 1996) which employs perturbed Coulomb functions for asymptotic solutions is able to analyse the Rydberg series for high members and here gives another perturber, 1s2p(^{3}P)6s, at 66.306 eV, close to the Rydberg members with $n \sim 30$. It is in full agreement with the analysis by Chung (1997a), which gives 66.309 eV for the energy position of this resonance.

4.3. Resonances in the 1s2s ^{1}S–1s2p ^{3}P energy region

Figure 3 compares our photoionization cross sections with the measurements by Kiernan *et al* (1996) in this energy region, and the comparison with other calculations is given in table 10. The experiment gives a relatively simple resonance structure with one dominating resonance

at 66.430 eV, which has been attributed to the 1s2p(^{1}P)4s state. Other weak structures are caused by the 1s2p(^{3}P)*n*s and 1s2p(^{3}P)*n*d Rydberg series, but our assignments for separate members in these series differ considerably from those suggested by Chung (1997a) and Vo Ky *et al* (1998). The cross section just above the 1s2s ^{1}S threshold has a well defined plateau, which is formed by the effect of two resonances, 1s2p(^{3}P)7s and 1s2p(^{3}P)7d. In general, the *n*s states have much broader widths and a different structure from the *n*d states. Then we see in the cross section a sharp strong peak which is assigned to the perturber 1s2p(^{1}P)4s. Its larger intensity can be understood because the dipole excitation without a change of spin is much more favoured, even in the case of strong configuration mixing. Up to now, our assignments coincide with those given by Chung (1997a), but the shoulder above the perturber is attributed by Chung (1997a) to the 1s2p(^{3}P)8s resonance. According to our calculations, there are no resonances in this region up to 66.465 eV where we have the 1s2p(^{3}P)8d state. We carefully analysed the eigenphase sum in this region and did not find any sharp changes of phases that would indicate a resonance. Our explanation is that the perturber so strongly interacts with the 1s2p(^{3}P)*n*s series that it shifts up the upper terms of this series, with a change of quantum defect of $\sim$1. This reverses the relative positions of the *n*s and *n*d terms in this energy region. The assignment given by Vo Ky *et al* (1998) has an additional shift of the quantum defect for the *n*d series and revised relative positions for the perturber and 1s2p(^{3}P)8s state. On the other hand, their values for energies of resonances in this region are in close agreement with our results.

The partial widths presented in table 10 show that the resonances in this region mainly decay to the excited states of Li^+, with the channel 1s2s(^{3}S)*k*p being the dominant channel. The resulting resonance structure is very weak in the total cross sections, but it is more clearly seen in the partial cross sections which are not presented here.

4.4. Resonances in the 1s2p ^{3}P–1s2p ^{1}P energy region

The resonance pattern in this energy region has the simplest structure (see figure 4 and table 11). There are no perturbers in this region and resonances regularly appear in the spectra as members of the 1s2p(^{1}P)*n*s and 1s2p(^{1}P)*n*d Rydberg series. Again, our photoionization cross section profiles and peak positions agree precisely both with experiment and calculations by Chung (1997a) and Vo Ky *et al* (1998). As noted by Chung (1997a), although the peak positions and the line profiles in theory agree closely with experiment, there is some discrepancy in the comparison of absolute values of cross sections. This discrepancy varies in the range of 20% for different energy regions. On the other hand, all the theoretical results discussed here agree closely in the energy region considered. Note also the regular behaviour of the partial and total autoionizing widths for the higher-lying members of the Rydberg series, with no dominant decay channel to be indicated. There are no data in the literature for comparison of autoionizing widths in this energy region.

4.5. Convergence of the close-coupling expansion

The close agreement between the 11-state *R*-matrix calculation of Lisini *et al* (1990), the 19-state *R*-matrix result of Vo Ky *et al* (1998) and experimental results in respect of all questions, which concern the total and partial photoionization cross sections at energies below the 1s2*l* excitation thresholds, indicates the convergence of the close-coupling expansion for these excitation parameters. However, as was shown above, there are some discrepancies in the description of the resonance structure. Therefore, we below present a more detailed view of

Table 11. Energies and total and partial widths of autoionization states in Li below the 1s2p ^{1}P threshold (67.607 eV).

	Energy (eV)			Width	Partial widths (%)				
State	Expt[a]	Calc.[b]	Calc.[c]	(meV)	$1s^2kp$	1s2s(^{3}S)kp	1s2s(^{1}S)kp	1s2p(^{3}P)ks	1s2p(^{3}P)kd
1s2p(^{1}P)4d	66.804	66.781	66.796	12.4	0.7	17.1	34.6	12.0	35.6
1s2p(^{1}P)5s	66.907	66.907	66.913	21.3	0.4	21.9	25.2	13.0	39.5
1s2p(^{1}P)5d	67.094	67.076	67.080	9.80	5.8	12.8	35.6	9.1	36.6
1s2p(^{1}P)6s	67.141	67.145	67.146	11.6	0.5	21.3	27.9	12.2	38.1
1s2p(^{1}P)6d	67.246	67.238	67.240	6.46	11.7	11.2	33.5	8.4	35.2
1s2p(^{1}P)7s	67.275	67.279	67.279	6.99	0.5	21.5	30.1	11.9	36.0
1s2p(^{1}P)7d		67.336	67.335	4.29	14.0	10.6	32.6	8.2	34.6
1s2p(^{1}P)8s	67.358	67.362	67.361	4.52	0.5	21.8	31.9	11.8	34.0
1s2p(^{1}P)8d		67.399	67.398	2.96	14.7	10.4	32.4	8.1	34.4
1s2p(^{1}P)9s	67.413	67.418	67.416	3.10	0.5	22.2	33.3	11.7	32.3
1s2p(^{1}P)9d		67.444	67.442	2.12	14.7	10.3	32.4	8.1	34.4
1s2p(^{1}P)10s	67.453	67.457	67.454	2.21	0.5	22.5	34.2	11.6	31.2
1s2p(^{1}P)10d		67.476	67.473	1.56	14.7	10.3	32.5	8.1	34.4
1s2p(^{1}P)11s	67.477	67.485	67.482	1.64	0.5	22.9	35.2	11.6	29.9
1s2p(^{1}P)11d		67.500	67.496	1.19	14.6	10.2	32.6	8.1	34.5
1s2p(^{1}P)12s	67.502	67.506	67.503	1.24	0.5	23.1	35.7	11.5	29.2
1s2p(^{1}P)12d		67.516	67.513	0.92	14.9	10.2	32.4	8.2	34.4
1s2p(^{1}P)13s	67.516	67.521	67.519	0.97	0.5	22.5	36.6	11.5	27.9

[a] Kiernan *et al* (1996), photoion spectra measurements (±0.010).
[b] Vo Ky *et al* (1998), 19-state *R*-matrix calculations.
[c] Present work.

the convergence of the close-coupling expansion with respect to resonance parameters such as energy positions and autoionizing widths.

Table 12 compares the energies and widths obtained from the four close-coupling calculations, 5CC, 11CC, 5CC* and 11CC*, which are carried out in the five- and 11-state *R*-matrix approximations, each with and without the inclusion of correlation functions. The asterisk indicates the inclusion of correlation functions as described in section 3.3.

For the lowest autoionizing states, as can be seen from table 12, the correlation functions give the dominant corrections, especially for the values of autoionizing widths. In this case the main correlation corrections arise from the short-range interaction, for which the convergence of the pure close-coupling expansion is slow. For the lowest state 1s(2s2p ^{3}P) ^{2}P^o, we also carried out the simple one-channel *R*-matrix calculations with a more extensive set of correlation functions, and obtained an energy of 58.919 eV and width of 3.33 meV. These values are very close to the 11CC* results that also suggests the importance of the short-range correlation in the study of low-lying autoionizing states. It is interesting to note in this respect that for high-lying members of this Rydberg series (see, for example, the results for the 1s2s(^{3}P)9p state in table 12), the energies obtained in different approximations are very close, but there are still considerable corrections for widths due to the inclusion of correlation functions. It has a simple explanation, because the autoionization process involves the inner electrons, for which the short-range corrections are important.

Now consider the autoionizing states placed between excited thresholds. Table 12 shows that in this case the main effect on the energies and widths gives the additional channels in the close-coupling expansions, though the effect of correlation functions is also noticeable. It is most clearly seen in the example of the 1s2p(^{1}P)4s perturber, for which the energies obtained

Table 12. Comparison of energies and widths in respect of the convergence of the close-coupling expansion for some selected $^2P^o$ autoionizing states in Li. 5CC and 11CC stand for the five- and 11-state R-matrix calculations, respectively. An asterisk indicates inclusion of the short-range correlation functions in the close-coupling expansion.

	Energies (eV)				Widths (meV)			
	5CC	11CC	5CC*	11CC*	5CC	11CC	5CC*	11CC*
$1s(2s2p)^3P$	58.956	58.937	58.930	58.923	4.88	4.49	3.60	3.48
$1s(2s2p)^1P$	60.517	60.454	60.443	60.419	10.1	9.86	9.81	9.54
$1s2s(^3S)3p$	62.435	62.427	62.427	62.423	0.148	0.158	0.200	0.196
$1s2s(^1S)3p$	64.060	64.052	64.056	64.051	0.409	0.421	0.301	0.352
$1s2s(^3S)9p$	64.233	64.232	64.233	64.232	0.089	0.074	0.054	0.058
$1s2s\ ^3S$	—							
$1s2p(^3P)3s$	64.594	64.578	64.589	64.570	108	115	110	113
$1s2s(^1S)4p$	65.182	65.150	65.172	65.147	78.9	87.5	74.6	84.2
$1s2p(^3P)3d$	65.285	65.258	65.280	65.257	27.3	19.0	26.4	19.3
$1s2p(^1P)3s$	65.327	65.299	65.316	65.296	5.68	2.95	4.67	2.82
$1s2p(^3P)4s$	65.578	65.568	65.573	65.566	71.3	68.1	68.4	66.3
$1s2s(^1S)5p$	65.677	65.671	65.674	65.670	4.94	3.79	3.99	3.27
$1s2s\ ^1S$	—							
$1s2p(^3P)7s$	66.359	66.357	66.358	66.356	10.11	9.590	9.558	9.487
$1s2p(^3P)7d$	66.405	66.402	66.404	66.402	0.714	0.956	0.798	0.941
$1s2p(^1P)4s$	66.435	66.432	66.433	66.432	1.35	0.317	1.009	0.336
$1s2p(^3P)8d$	66.467	66.465	66.466	66.464	0.784	0.501	0.547	0.469
$1s2p\ ^3P$	—							
$1s2p(^1P)5s$	66.806	66.792	66.803	66.790	11.70	12.24	11.62	12.38
$1s2p(^1P)5d$	66.920	66.911	66.918	66.911	21.32	21.63	21.40	21.29
$1s2p\ ^1P$	—							

in the different approximations are very close, but the widths differ considerably. As was shown in the preceding sections, it is particularly important for these states to correctly include the interaction between different Rydberg series, and the accurate representation of the target wavefunctions plays an important role here.

As a whole, we may conclude that the 11-state approximation with the correlation functions used in the present work includes all the important correlation effects which are necessary for a correct representation of the resonance structure in the Li photoionization.

5. Summary

We have introduced a new extended version of the R-matrix method for the calculation of continuum properties. The main innovation in comparison with a standard R-matrix approach consists in the introduction of non-orthogonal orbitals to describe both the target states and the R-matrix basis functions. It considerably extends the capabilities of the R-matrix technique and puts at our disposal a greater flexibility in the choice of the target wavefunctions. This possibility is very important in the case of complex atoms where a strong dependence of the one-electron radial functions on the configuration terms is often encountered. The non-orthogonal technique also allows the R-matrix basis functions to be chosen from any appropriate complete set, without restrictions on orthogonality conditions which are usually imposed in scattering calculations.

In the present computational implementation, the continuum orbitals in the inner region are described in terms of B-splines, due to their excellent numerical properties. Using a Bloch operator, for which an analytic expression in the B-spline basis is known (van der Hart 1997), a good description of the electron flux through the boundary can be obtained while maintaining the Hermiticity of the inner region matrix. The completeness of the B-spline basis ensures that no Buttle correction to the R-matrix elements is required, and a lot of computational time may be saved. For a compete description of the scattering process we also need the asymptotic solutions in the outer region which can be easily found by using the well developed standard R-matrix outer region codes, such as for example the FARM program by Burke and Noble (1995) or the ASYPCK program by Crees (1980), depending on the task at hand.

The present introduction of the non-orthogonal technique into the scattering calculations became possible after the development of general and efficient codes (Zatsarinny 1996, Zatsarinny and Froese Fischer 1999) for computation of the atomic structure matrix elements on the basis of non-orthogonal orbitals. In general, the non-orthogonal technique leads to much more time-consuming calculations in comparison with orthogonal orbitals. On the other hand, the non-orthogonal approach allows us to employ more compact configuration expansions for target wavefunctions and the bound part of the total scattering function, with the same level of accuracy. In addition, the above-mentioned angular programs allow one to create data banks for matrix elements that may considerably reduce the computational effort. As a whole, the overall computational effort is not increased noticeably in comparison with the standard R-matrix calculations.

Another advantage of the present approach is that the correlation $(N + 1)$-electron bound configurations, which are used for the description of the short-range correlation, can be introduced naturally into the close-coupling expansion, with great flexibility in their choice. Consequently, the present approach is totally free of the problem of pseudo-resonances, which arise from an inconsistent description of the scattering and bound parts of the total wavefunction, and which for a long time have plagued many close-coupling calculations in the case of complex atoms.

The effectiveness of the present approach has been demonstrated by exploring the resonance structure in the Li photoionization cross sections. The availability of accurate experimental results for lithium enabled the theoretical models to be tested in a detailed way. We present the detailed description of the resonances in the energy range of the 1s2l excitation thresholds by using an 11-state R-matrix approximation, and discuss the convergence of the close-coupling expansion. The close agreement with the high-resolution measurements by Kiernan *et al* (1996) indicates the high accuracy of the present approach. A considerable improvement of the resonance description has been achieved in comparison with the standard 19-state R-matrix calculations by Vo Ky *et al* (1998). It can be attributed to the more accurate description of target states and to the inclusion of short-range correlation in our calculations. Excellent agreement has been found with the sophisticated results of Chung (1997a, b) which were obtained by using the saddle-point complex-rotation method. This method exploits the total wavefunctions with very complicated structure, which can hardly be extended to more complex atoms. On the other hand, the proposed approach and the related computational technique can be applied directly to more complex many-electron systems with a similar level of computational effort.

Acknowledgments

The present study was supported in part by the International Soros Science Education Programme of the International Renaissance Foundation, grant QSU082069. The research

of one of the authors (CFF) was supported by the Division of Chemical Sciences, Office of Basic Energy Sciences, Office of Energy Research, US Department of Energy.

References

Armen G B, Craig B I, Larkins F P and Richards J A 1990 *J. Electron Spectrosc. Relat. Phenom.* **51** 183
Armen G B and Larkins F P 1991 *J. Phys. B: At. Mol. Opt. Phys.* **24** 2675
Accad Y, Pekeris C L and Schiff B 1971 *Phys. Rev.* A **4** 516
Bartschat K 1998 *Comput. Phys. Commun.* **114** 168
Bartschat K and Burke P G 1986 *Comput. Phys. Commun.* **41** 75
Berrington K A, Eissner W B and Norrington P N 1995 *Comput. Phys. Commun.* **92** 290
Brage T, Froese Fischer C and Miecznik G 1992 *J. Phys. B: At. Mol. Opt. Phys.* **25** 5289
Bray I and Stelbovics A T 1995 *Comput. Phys. Commun.* **85** 1
Burke P G and Berrington K A ed 1993 *Atomic and Molecular Processes: an R-matrix approach* (Bristol: IOP Publishing)
Burke P G, Hibbert A and Robb W D 1971 *J. Phys. B: At. Mol. Phys.* **4** 153
Burke P G and Seaton M J 1971 *Methods Comput. Phys.* **10** 1
Burke V M and Noble C J 1995 *Comput. Phys. Commun.* **85** 471
Busby D W, Burke P G, Burke V M, Noble C J and Scott N S 1999 *Comput. Phys. Commun.* **114** 243
Buttle P J A 1967 *Phys. Rev.* **160** 719
Chung K T 1991 *Phys. Rev.* A **44** 5421
——1997a *Phys. Rev. Lett.* **78** 1416
——1997b *Phys. Rev.* A **56** R3330
Crees M A 1980 *Comput. Phys. Commun.* **19** 103
Crees M A, Seaton M J and Wilson P M H 1978 *Comput. Phys. Commun.* **15** 23
de Boor C 1985 *A Practice Guide to Splines* (New York: Springer)
Ederer D L, Lucatorto T and Madden R P 1970 *Phys. Rev. Lett.* **25** 1537
Ferrett T A, Lindle D W, Heimann P A, Brewer W D, Becker U, Kerkhoff H G and Shirley D A 1987 *Phys. Rev.* A **36** 3172
Froese Fischer C, Brage T and Jönsson 1997 *Computational Atomic Structure. An MCHF Approach* (Bristol: IOP Publishing)
Froese Fischer C, Guo W and Shen Z 1992 *Int. J. Quant. Chem.* **42** 849
Froese Fischer C and Idrees M 1989 *Comput. Phys.* **3** 53
Gorczyca T W, Robicheaux F and Pindzola M S 1995 *Phys. Rev.* A **52** 3877
Hansen J E, Bently M, van der Hart H W, Landtman M, Lister G M S, Shen Y-T and Vaeck N 1993 *Phys. Scr.* T **47** 7
Henry R J W, Rountree S P and Smith E R 1981 *Comput. Phys. Commun.* **23** 233
Hibbert A 1970 *Comput. Phys. Commun.* **1** 359
Hibbert A and Froese Fischer C 1991 *Comput. Phys. Commun.* **64** 417
Hibbert A, Glass R and Froese Fischer C 1991 *Comput. Phys. Commun.* **64** 455
Hudson R D and Carter V L 1967 *J. Opt. Soc. Am.* **57** 651
Kiernan L M, Lee M-K, Sonntag B F, Sladeczek P, Zimmermann P, Kennedy E T, Mosnier J-P and Costello J T 1996 *J. Phys. B: At. Mol. Opt. Phys.* **29** L181
Kupliauskiene A 1996 *Phys. Scr.* **53** 149
Langer B, Viefhaus J, Hemmer O, Menzel A and Wehlitz R 1991 *Phys. Rev.* A **43** 1652
Larkins F P, Adeney P D and Dyall K G 1981 *J. Electron Spectrosc. Relat. Phenom.* **51** 183
Li J M, Vo Ky L, Qu Y Z, Yan J, Zhang P H, Zhou H L and Faucher P 1997 *Phys. Scr.* A **55** 3239
Lisini A, Burke P G and Hibbert A 1990 *J. Phys. B: At. Mol. Opt. Phys.* **23** 3767
Mannervik S and Cederquist H 1985 *Phys. Scr.* **31** 79
McKenzie D K and Drake G W F 1991 *Phys. Rev.* A **44** 6973
Mehlman G, Ederer D L, Saloman E B and Cooper J W 1978 *J. Phys. B: At. Mol. Phys.* **11** L689
Pedrotti K D 1987 *Opt. Commun.* **62** 250
Quigley L and Berrington K 1996 *J. Phys. B: At. Mol. Opt. Phys.* **29** 4529
Quigley L, Berrington K and Pelan J 1998 *Comput. Phys. Commun.* **114** 225
Saha H P and Lin D 1997 *J. Phys. B: At. Mol. Opt. Phys.* **30** 1651
Sapirstein J and Johnson W R 1996 *J. Phys. B: At. Mol. Opt. Phys.* **29** 5213
Schiff B, Pekeris C L and Accad Y 1971 *Phys. Rev.* A **4** 885
Stibbe D T and Tennyson J 1998 *Comput. Phys. Commun.* **114** 236

Tennyson J and Noble C J 1984 *Comput. Phys. Commun.* **33** 421
van der Hart H W 1997 *J. Phys. B: At. Mol. Opt. Phys.* **30** 453
Venuti M and Decleva P 1997 *J. Phys. B: At. Mol. Opt. Phys.* **30** 4839
Vo Ky L, Faucher P, Hibbert A, Li J-M, Qu Y-Z, Yan J, Chang J C and Bely-Debau F 1998 *Phys. Rev.* A **57** 1045
Xi J and Froese Fischer C 1999 *Phys. Rev.* A **59** 307
Zatsarinny O 1996 *Comput. Phys. Commun.* **98** 235
Zatsarinny O and Froese Fischer C 1999 *Comput. Phys. Commun.* at press